INTERNATIONAL JOURNAL OF AUTOMOTIVE AND MECHANICAL ENGINEERING
ISSN: 2229-8649 e-ISSN: 2180-1606
VOLUME 22, ISSUE 4, 2025, 12903 - 12919
DOI: https://doi.org/10.15282/ijame.22.4.2025.5.0982

RESEARCH ARTICLE

Evaluation of Naca 4412 and Clark-Y Aerofoil Based Drone Propellers' Efficiencies Fabricated Using Additive Manufacturing

Muhammad Nor Ikmal Muhamad Nazri[1]*, Adi Azriff Basri[1,2,3] ,Mohd Na'im Abdullah[1], Faizal Mustapha[1], Farid Bajuri[1], Ernnie Illyani Basri[1] and Nasrul Hadi Johari[4]

[1]Department of Aerospace Engineering, Faculty of Engineering, Universiti Putra Malaysia, 43400 Serdang, Selangor, Malaysia

[2]Aerospace Malaysian Research Center, Universiti Putra Malaysia, 43400 Serdang, Selangor, Malaysia

[3]Laboratory of Biocomposite Technology, Institute of Tropical Forestry and Forest Products, Universiti Putra Malaysia, 433400 Serdang, Selangor, Malaysia

[4]Centre for Advanced Industrial Technology, Universiti Malaysia Pahang Al-Sultan Abdullah, 26600 Pekan, Pahang, Malaysia

ABSTRACT – The widespread use of drones has garnered considerable attention, given their diverse range of feasible applications and the modest costs required for operation. Yet, materials for drone propellers have not been widely explored. The proper usage of materials and the selection of additive manufacturing for structurally complex aerodynamic blade designs in drones' design and development provide compelling energy savings. This work presents a 3D printed propeller using Fused Deposition Modelling (FDM) and Stereolithography (SLA) based on Acrylonitrile Butadiene Styrene (ABS) and Polylactic Acid (PLA). ABS resin is the most preferred manufacturing method for propellers, with 9.6% more ductility compared to ABS filament and PLA resin, as indicated by the stress-strain curve obtained through the tensile test. A static test experiment was conducted on an ABS resin-based 3D printed propeller to compare the propeller performance between NACA 4412 and Clark-Y. From the experiment, with the same diameter and pitch, NACA 4412 was proven to be more efficient compared to Clark-Y, with 15.86% higher static thrust and 9.32% higher efficiency. The significant findings from the 3D-printed propeller are derived from the aerodynamic parameters that influence thrust, power, and efficiency. Thus, this study lays the groundwork for achieving optimal propeller performance, particularly from an additive manufacturing perspective.

ARTICLE HISTORY

Received	:	07th Aug. 2024
Revised	:	05th May 2025
Accepted	:	12th June 2025
Published	:	15th Nov. 2025

KEYWORDS

3D printing
Fused Deposition Modelling (FDM)
Stereolithography (SLA)
Acrylonitrile Butadiene Styrene (ABS)
Polylactic Acid (PLA)
Drone propellers

1. INTRODUCTION

Drones, also known as Unmanned Aerial Vehicles (UAVs), have undergone significant technological advancements and have experienced rapid growth in recent years, with a wide range of applications across various industries. The evolution of drone technology has emerged from the early development of simple remote-controlled aircraft to sophisticated unmanned systems with advanced capabilities. The usage of drones has advanced from remote-controlled applications to autonomous flight, driven by advances in computing power and sensors, as well as miniaturisation and mobility. This evolution has led to the incorporation of advanced features for complex tasks, enhancing accuracy and safety. The wide range of applications of drones across various industries includes photography and videography, surveying and mapping, delivery services, agriculture, disaster management, and infrastructure applications.

Drone technology has garnered significant attention in research perspectives, encompassing extensive areas of study, particularly in technology and design development. Research on drones primarily focuses on improving flight dynamics [1-6], battery life [7-16], payload capacity [17-23], and sensor technology [24-28]. In addition, factors affecting the flight performance and capabilities of drones have also gained interest in research studies, particularly aerodynamics [29-37], propellers[38-40], weight and balance [41], power systems [42-47], and control systems [48-52]. Propellers are one of the crucial components that generate thrust and lift for drones. Factors that impact propeller performance include size, pitch, number of blades, and material composition, all of which are subject to the desired flight characteristics, payload requirements, and power system specifications of the drones.

The key factors that affect propeller performance are: (i) Size of the propeller, which is generally based on the weight of the drone and the specification of the motor for optimal performance. While the diameter of the propeller influenced the thrust generated, specifically, larger propellers generally generate more thrust. However, they need more power to rotate. (ii) Pitch is also another important element for a propeller as it generates forward thrust per revolution. A higher pitch will produce a higher distance per revolution, which means that a higher pitch will create higher forward speed when rotated at the same revolution per minute compared to a lower pitch propeller. However, to produce the same revolution per minute, more torque and power are required. (iii) The number of blades on the propeller affects its efficiency and thrust characteristics. Two-bladed propellers commonly provide a good balance between efficiency and performance. Three- or four-bladed propellers provide better stability and manoeuvrability at the cost of efficiency,

*CORRESPONDING AUTHOR | M. N. I. M. Nazri | ✉ ikmalnazri2000@gmail.com

subject to energy usage. (iv) The material composition of propellers is commonly made of plastic or composite materials, in which lightweight and rigid materials offer great performance and durability.

There is an emerging trend towards the use of additive manufacturing (AM), commonly known as 3D printing, particularly for the manufacturing of UAV or drone structures. The capability of AM can be associated with the production of lightweight and highly complex geometries with minimal tooling [53]. Conventional manufacturing methods such as drilling, lathing, and machining for metals and moulding for composites and plastics, require a lot of labour and offer less design freedom. There are various types of techniques in AM, namely stereolithography (SLA), selective laser sintering (SLS) and fused deposition modelling (FDM) for polymer and composite systems [54-55]. In order to achieve the lightweight characteristic of propeller structures under realistic loads, it is important to determine the material properties of the additively manufactured materials. It should be noted that the use of 3D-printed propellers has received less attention in research. However, this manufacturing method can be used for complex geometries and structural integrity of propellers to achieve the required aerodynamic performance. Several researchers have studied the suitability of using AM for UAV components. For example, 3D printing materials are mostly being tested for their use in UAV frames, wings, landing gear, motors and wheels[56-60].

The aim of this paper is to investigate the aerodynamic performance of a 3D printed propeller using different 3D printing techniques. The propeller is fabricated using SLA and FDM 3D printers for two types of material, namely ABS and PLA, in the form of resin and filament, in order to determine the respective mechanical properties of the material. PLA is a thermoplastic polyester made from renewable resources such as sugar cane or starch and, unlike the petrochemical plastics, is readily biodegradable [61]. On the other hand, ABS is also a thermoplastic that is often chosen due to its structural stability, durability and good corrosion, impact, wear and chemical resistance [62-63]. In this study, the material with the best mechanical properties is selected to design and fabricate two different airfoils, namely, Clark-Y and NACA 4412, prior to performing static tests to investigate the aerodynamic performance of the airfoils.

2. METHODS AND MATERIAL

The flowchart of this study is depicted in Figure 1. This study is conducted based on several phases, starting with the fabrication of samples for tensile tests and conducting these tests to select the best material for the propellers. Then, the propellers are designed and fabricated using the selected material. Finally, static tests are carried out on the fabricated propellers to analyse the aerodynamic performance of the chosen design using the 3D printed material. However, if the static test shows unacceptable aerodynamic performance, the propellers are required to be fabricated again and undergo the static test.

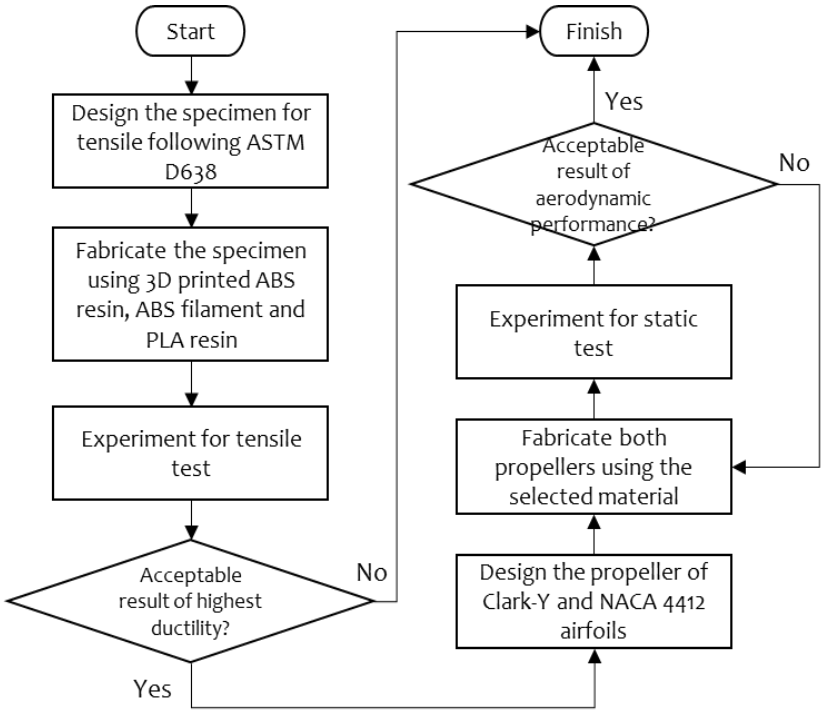

Figure 1. Flowchart of 3D printed propeller model

2.1 Tensile Test on 3D Printed ABS and PLA

2.1.1 Preparation of specimens

The materials used to fabricate the tensile specimens were Magma DuraABS tough resin (ABS resin), Flashforge's ABS filament and e-Sun's PLA resin. The properties of the materials provided by the supplier are summarised in Table

1. The tensile specimens are designed following the standard of ASTM D638 using SolidWorks computer-aided design software, as shown in Figure 2. The thickness of the specimen is 3.2 mm.

Table 1. Material properties of PLA and ABS used in this work as obtained by the supplier

Properties	Materials		
	Resin		Filament
	ABS	PLA	ABS
Viscosity (mPa.s)	200-350	100-270	-
Density (g/cm^3)	1.05-1.13	1.07-1.10	1.04
Tensile strength (MPa)	42-62	24-55	43
Elongation at break (%)	11- 21	24-37	22
Flexural strength (MPa)	60-80	25-61	66
Impact strength (J/m)	60-80	27-40	-
Heat distortion temperature (℃, 0.45 MPa)	-	-	78
Melt flow index (g/10 min)	-	-	12 (220℃/10kg)
IZOD Impact strength (kJ/m^2)	-	-	29
Hardness (Shore D)	75-80	75-82	-

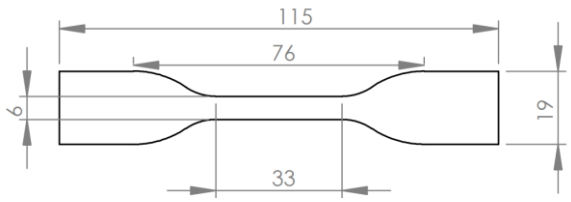

Figure 2. Tensile specimen dimension (unit: mm)

The machines used to print the specimens were Zortrax M200 and Creality LD-002R for FDM and SLA printing, respectively. ABS filament is printed using the Zortrax M200 printer, while ABS resin and PLA resin are printed using the Creality LD-002R printer. The design part files from SolidWorks are imported in STL format into the 3D printing software for the respective slicer of the printer. The Z-suite software is used to slice the 3D file for the Zortrax M200, as shown in Figure 3(a). For the Creality LD-002R, the 3D files are sliced using Chitubox, as shown in Figure 3(b). The ABS filament is printed horizontally, as in Figures 3(a) and 3(c). This increases the adhesion of the filament to the printer bed. On the other hand, both ABS and PLA resins are printed vertically, as depicted in the Figures. 3(b), 3(d)and 39(e). In contrast to the Zortrax M200 printer with a build volume of 200 mm × 200 mm × 180 mm, the Creality LD-002R printer had a smaller build volume of 119 mm × 65 mm × 160 mm, which meant that the tensile specimen could not fit horizontally on the built plate. As such, both ABS and PLA resins are printed vertically instead.

Both printers are set to an infill density of 100%. The layer height of the Zortrax M200 was 0.19 mm, while the layer height of the Creality LD-002R was 0.10 mm. For the specimens printed with Zortrax M200, the additional parts were trimmed with a clipper and smoothed with sandpaper. The specimens printed using Creality LD-002R are then post-cured under sunlight for about 3 hours before use.

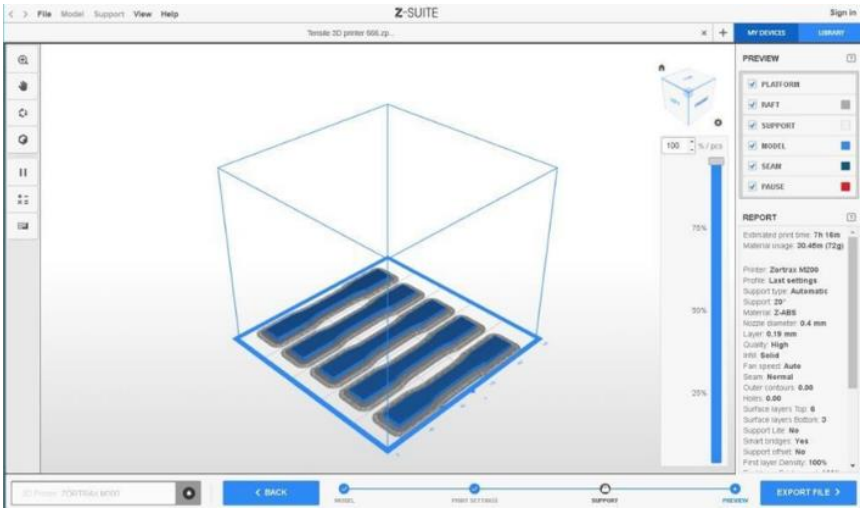

(a) Z-suite slicer used for Zortrax M200

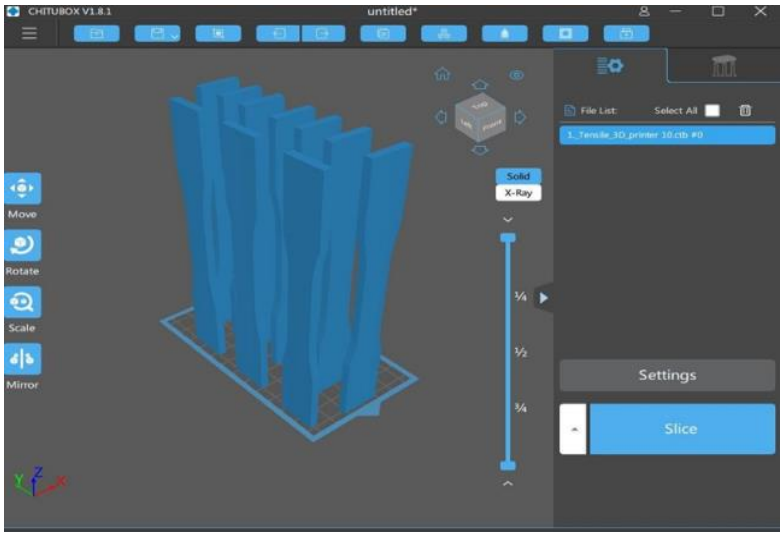

(b) Chitubox slicer used for Creality LD-002R

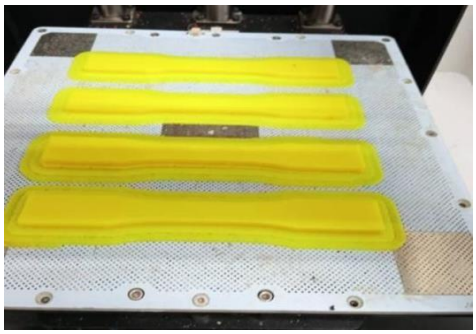

(c) ABS tensile specimen using Zortrax M200

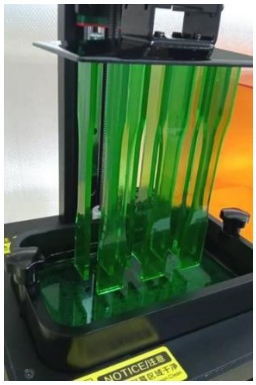

(d) ABS tensile specimen using Creality LD-00R

(e) PLA tensile specimen using Creality LD-002R printer

Figure 3. Software interfaces and 3D printing machines used in tensile sample preparation

2.1.2 Experimental setup for tensile test

The tensile test is conducted according to ASTM D638-10 standard test for tensile properties of plastics. In this experiment, seven specimens of each material are tested by clamping the wider part of the specimen to promote failure within the thin part. The tensile tests are performed using a 5kN Instron series model 3382 Universal Testing Machine. The crosshead speed was set to 5 mm/min with a strain rate of 0.1/min. An axial extensometer is used to analyse the strain. The tensile test is conducted as depicted in Figure 4. The analysis is based on the tensile strength, the modulus and the stress-strain curve obtained from the tests conducted. An average of five specimens is used for the analysis, with specimens where failure occurred near the wider section or specimens that tended to contribute to a high coefficient of

variation being considered as outliers. From the tensile test results, a material is selected for the fabrication of the propeller.

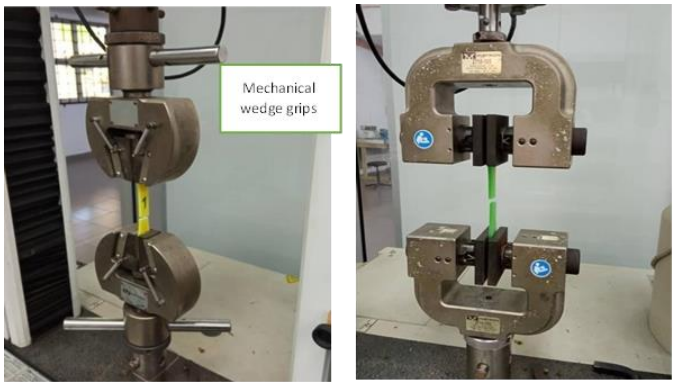

ABS filament specimen ABS resin specimen

Figure 4. Tensile test experiment

2.2 Static Test on Propeller based on Selected Material

2.2.1 Design and fabrication of propeller

The propellers were designed using the Airfoil Plotter from Airfoil Tools and Solidworks® 2016 software. In this study, two 4.2 × 4 (propeller with a diameter of 4.2 inches and a pitch of 4 inches/revolution) two-bladed propellers are designed using NACA 4412 airfoil for the first propeller and a Clark-Y airfoil for the second propeller [64]. The NACA 4412 and Clark-Y airfoils were chosen because they are frequently referenced in the literature, which facilitates the comparison and validation of the results. The geometry of the propeller blade was created referring to the APC Free Flight Propeller from the University of Illinois at Urbana-Champaign (UIUC) Propeller Data Site [65].

The geometry of both propellers was also obtained from the UIUC Propeller Data Site and summarized in Table 2 [66]. From Table 2, the geometry of the propeller, such as radius distribution (r/R), chord distribution (c/R), pitch angle (Beta/°), radius and chord length, can be compared for each section.

Table 2. APC Free Flight propeller geometry (Deters, 2015)

Radius distribution, r/R	Chord distribution, c/R	Pitch angle [Beta/°]	Radius [mm]	Chord [mm]
0.15	0.2027	38.363	8.001	10.812020
0.20	0.1909	42.864	10.668	10.182610
0.25	0.1865	45.208	13.335	9.947910
0.30	0.1823	44.502	16.002	9.723882
0.35	0.1800	42.724	18.669	9.601200
0.40	0.1817	40.263	21.336	9.691878
0.45	0.1860	37.416	24.003	9.921240
0.50	0.1895	34.613	26.670	10.107930
0.55	0.1902	32.197	29.337	10.145270
0.60	0.1880	30.083	32.004	10.027920
0.65	0.1830	28.195	34.671	9.761220
0.70	0.1750	26.509	37.338	9.334500
0.75	0.1642	24.943	40.005	8.758428
0.80	0.1506	23.468	42.672	8.033004
0.85	0.1341	21.855	45.339	7.152894
0.90	0.1145	19.775	48.006	6.107430
0.95	0.0855	17.162	50.673	4.560570
1.00	0.0090	15.732	53.340	0.480060

For the first propeller, the NACA 4412 airfoil geometry is applied to all sections. By implementing the geometry values in Airfoil Tools, the plotted airfoil is then converted to CSV coordinates, which are tabulated in Microsoft Excel for further adjustment. Table 3 summarises the parameters of NACA 4412 and Clark-Y. Figure 5 illustrates the NACA 4412 airfoil with the desired geometry. The same method is repeated for the second propeller using the Clark-Y airfoil, as shown in Figure 6.

Table 3. Parameters of NACA 4412 and Clark-Y aerofoils [67]

Parameters	NACA 4412	Clark-Y
Max Thickness [%]	12	11.7
Chord at max thickness [%]	30	30.9
Max Camber [%]	4	3.4
Chord at max camber [%]	40	43.5
Trailing edge angle [°]	14.4	15.3
Lower flatness [%]	76.1	71.8
Leading edge radius [%]	1.2	1.2
Max lift coefficient	1.507	1.295
Angle of max lift coefficient [°]	11	8.5
Max Lift/Drag ratio	57.209	51.615
Max Lift/Drag angle	5.5	7
Max Lift/Drag lift coefficient	1.188	1.18
Stall angle [°]	6	8.5
Zero lift angle [°]	-4	-3.5

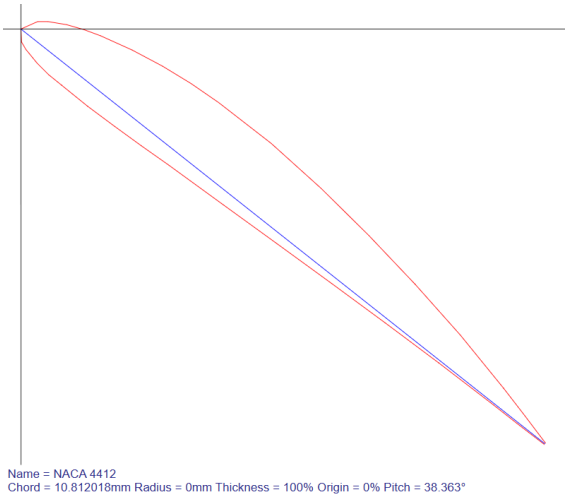

Figure 5. Plotted NACA 4412 aerofoil from airfoil tools

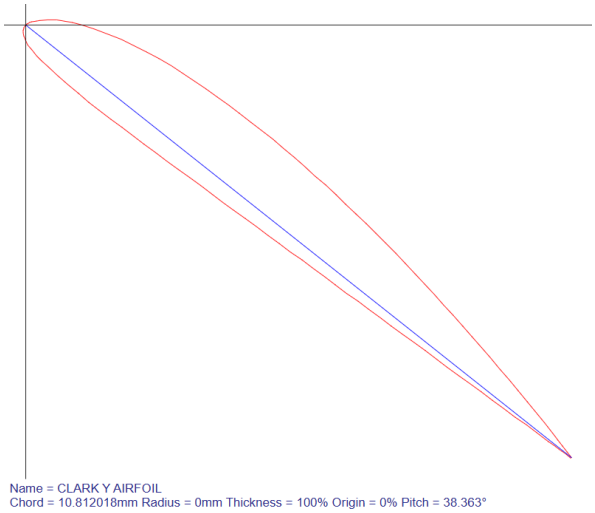

Figure 6. Plotted NACA Clark-Y aerofoil from Airfoil Tools

The CSV coordinate files are only tabulated in the coordinates of the y- and z-axis of the airfoil. The x-axis is added to all sections before the file is saved in .text format. The propeller design is drawn in a plane-to-plane section. The curve function in the Solidworks® 2016 software is used to insert the saved airfoil coordinate file. Then, the lofted boss/base feature is applied, connecting the curve on the plane section by section to create a solid drawing. The final design is shown

in Figures 7 and 8. As with the tensile specimens, the drawing is converted to STL file format and then sliced using the Chitubox software, as the chosen material for the propellers was ABS resin (the reason for using this material is discussed in the results section). The propellers are printed using the Creality LD-002R 3D printer, using the same settings as for the tensile specimens.

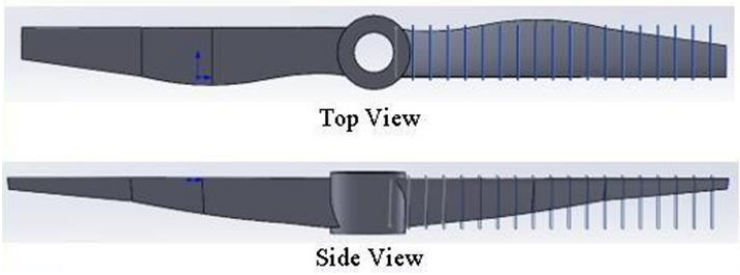

Figure 7. NACA 4412 propeller

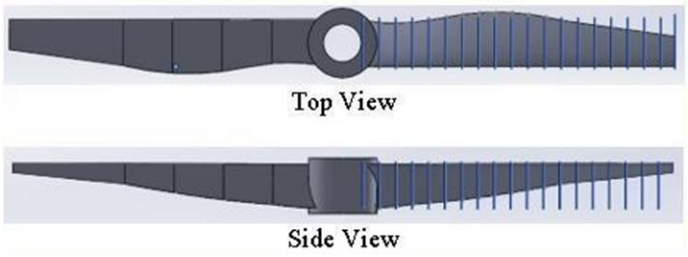

Figure 8. Clark-Y propeller

2.2.2 Experimental setup of static test

To investigate the performance of the propeller, it is important to conduct static and advanced flow analysis. In this study, the static test is performed using a Mayatech MT10-PRO test rig, which is made of CNC-processed metal, equipped with a motor mounting seat, XT60 plug, load cell, LCD screen with galvanometer display and has a thrust measurement range of 0-10 kg. The upper LCD screen displays the current, voltage and power consumed by the motor. The static test rig is shown in Figure 9.

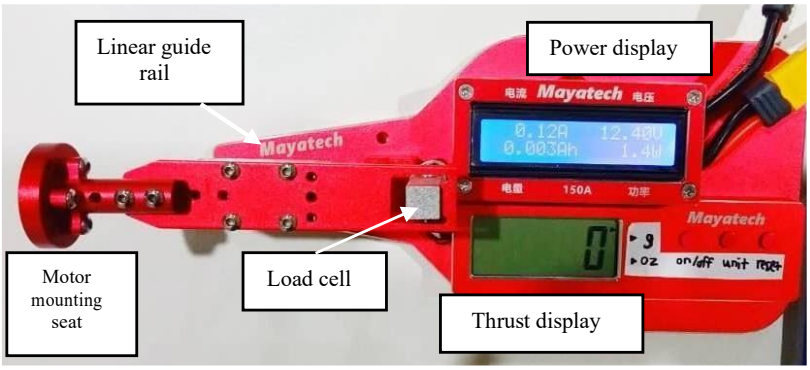

Figure 9. Mayatech MT10-PRO static test rig

From Figure 9, the load cell acts as a transducer that converts a force, such as tension, into a measurable electrical output. The electrical signal changes proportionally to the force exerted on the load cell. A micro linear guide rail connects the load cell and the motor. Other essential components of this setup include a Skywalker 40A electronic speed controller (ESC), a set of DS-6A transmitters, a Turnigy 3s 2650 mAh Lipo battery and a 2450 kV Racestar brushless motor with a locking mechanism. The transmitter sends the signal to the receiver, which passes the command to the ESC to control the speed of the motor according to the throttle movement.

The setup for the static test is shown in Figure 10. Since the propeller rotates at high speed and vibrates uncontrollably during the static test, safety precautions are required in the event of a propeller failure. A safety box is built to contain the shattered propeller in the event of catastrophic failure to prevent unwanted injuries. In addition, the propeller enclosure is placed approximately 4 cm away from the base to allow for the upstream and downstream airflow. The motor is properly mounted on the motor mounting seat of the test rig. A reflective tape is attached to the propeller to measure revolutions per minute (RPM). Then, the propeller is tightened into the motor until the locking mechanism can be unlocked by hand. A tachometer is used to measure the RPM of the propeller during the static test. A hole is cut in front of the safety box to

allow the laser to pass through for the RPM measurement. With the same setup and instruments used in this experiment, the test can easily be repeated in the future.

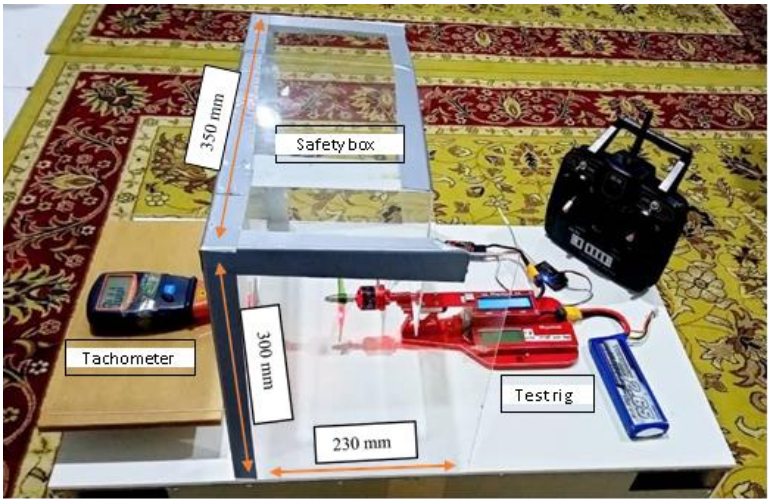

Figure 10. Full static test setup

2.2.3 Measurement of propeller speed and thrust

The initial preparation of the static test is conducted by connecting the battery, ESC, receiver and motor and ensuring that they are connected correctly. For the static test, the load cell is reset until the thrust display shows a value of zero. Using the DS-6A transmitter, the throttle stick is adjusted and trimmed to zero percent. The tachometer is aligned so that it points toward the reflective tape on the propeller surface. The static test rig rotated the propellers while the tachometer measured the RPM of the propeller attached to the test rig. The power required to rotate the propeller at a particular RPM is recorded, as is the thrust generated by the propeller.

To start the static test, the throttle stick of the ESC is pushed up until the propeller starts to rotate. The measurement of thrust and RPM starts with the lowest value of the RPM measurement. Starting from the lowest RPM value, the corresponding thrust value is recorded in the display. Then, the throttle is pressed further to the desired RPM value, such as 2000, 3000, 4000 RPM onwards, with a constant increment until the maximum RPM of the propeller or the maximum limit of the throttle has been reached. All the RPM and thrust data are collected and tabulated to analyse the propeller performance based on efficiency (η). The efficiency can be calculated using the momentum-blade element theory as shown in Eq. (1) to Eq. (3) [67], where C_T is the coefficient of thrust, C_P is the coefficient of performance, n is the rotational speed in rev/s, D is the propeller diameter in meters, and ρ is the density of the air in kg/m^3. The density of air in the equation is assumed to be the standard air density of 1.225 kg/m^3.

$$C_T = \frac{T}{\rho n^3 D^4} \tag{1}$$

$$C_P = \frac{P}{\rho n^3 D^5} \tag{2}$$

$$\eta = \frac{C_T}{C_P} \tag{3}$$

3. RESULTS AND DISCUSSION

3.1 Tensile Test Results

The result is presented in the form of strength, modulus and stress versus strain curve. As can be seen in Figures 11 to 13, most of the specimens broke in the centre area of the specimen. The validity of the test is based on the repeatability of at least five specimens. Specimens with failure near the wide section of the specimen, such as sample number 9 of the ABS resin, are considered outliers and removed from the data analysis.

Figure 11. Condition of specimens after tensile test for the ABS filament specimen

Figure 12. Condition of specimens after tensile test for the ABS resin specimen

Figure 13. Condition of specimens after tensile test for the PLA resin specimen

The tensile strength is the maximum strength that the specimen achieves before the strength weakens and fails. On the other hand, the tensile modulus or Young's modulus represents the stiffness or rigidity of a material. The tensile modulus is a quantity that indicates the ability of a material to withstand a force before it deforms. Figure 14 shows the tensile strength and modulus of the tested specimens. At 40 MPa and 4.07 GPa, ABS filament shows the highest strength and modulus compared to the other materials, followed by PLA resin and ABS resin. In terms of strength and modulus perspective, PLA filament can be considered the most suitable material. However, it should be noted that FDM-based printing produces anisotropic products. This is due to the material itself and the printing method. The FDM printer first prints the outermost layers (shells) of the model and then fills the inside (infill) with filaments by overlaying the previously printed layers [68]. The shells provide the shape and surface of the model and contribute to the structural integrity of the model, while the infill provides internal support and prevents the model from being hollow or fragile [69]. As the infill is printed in the chosen pattern, the structural properties of the shells and infills vary, making the model itself anisotropic. It has been shown that SLA-printed specimens are isotropic compared to highly anisotropic FDM-printed specimens, as there are no interfaces between the layers due to the same curing process of the resin, which leads to bonding between layers[70]. Therefore, the results shown in Figure 14 for ABS resin and PLA resin are similar for he stresses at different angles, while the value for ABS filament can be significantly lower or higher depending on the printing condition.

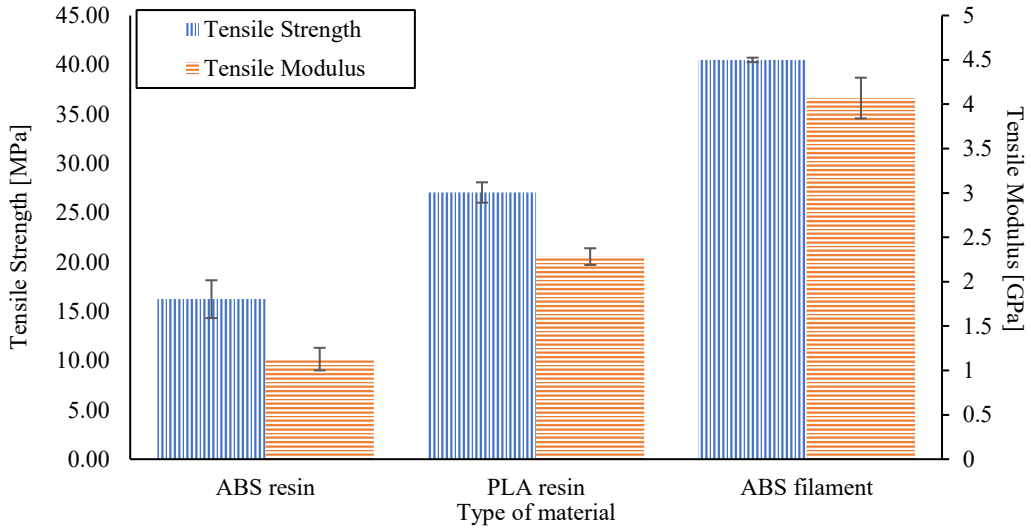

Figure 14. Tensile strength and modulus of the tested specimens

Figure 15 presents the general stress-strain curve for each type of material. The deformation of polymers is divided into two parts: elastic and plastic deformation. Elastic deformation is attributed to the linear regression section in the stress-strain curve at lower strain, where the polymer returns to its original shape after the load is removed. In Figure 15, the ABS filament has the greatest elasticity, while PLA resin and ABS resin show hardly any elasticity. At the end of elastic deformation, the polymer yields and goes into plastic deformation, where it does not return to its original shape after the load is released. The stress-strain curve of the ABS filament shown in Figure 15 agrees with the study by Cosmi et al. [70] in which the ABS filament failed when reaching the yield point and a maximum stress before failure. For PLA resin and ABS resin, the stress-strain curve shows plastic deformation with the highest strength at the breaking point. This curve pattern is similar to Cosmi et al. [70]. ABS resin fails at a significantly higher strain compared to both ABS filament and PLA resin.

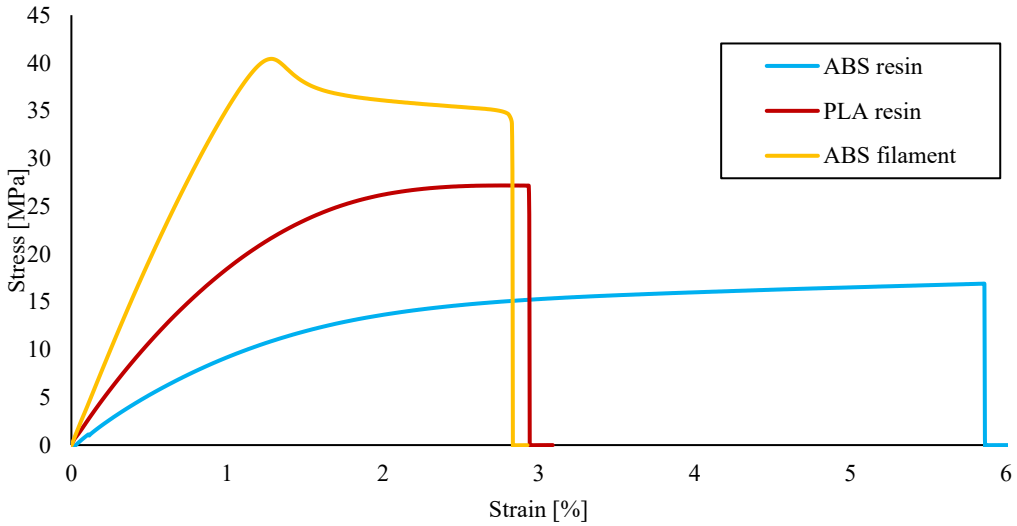

Figure 15. General stress-stain curve for each type of material

While ABS resin has lower strength, the post-curing regimen used in this work may not be the most suitable for SLA-based resin. Riccio et al. [71] reported that post-curing of SLA samples with 405 nm ultraviolet (UV) light at elevated temperature (60-80°C) strengthened the materials the most, but at the cost of increased brittleness. Exposure to UV light improves mechanical strength by forming additional chemical bonds that solidify the resin, while increasing the temperature helps to accelerate the process [72]. In this work, UV light is not available, so the sample is exposed to sunlight to promote the post-curing process [73]. However, the UV radiation of sunlight is in the range of 100-400 nm, and the specimens are exposed to a temperature of about 30°C [74]. This means that the SLA-printed specimens produced in this work did not receive the optimal post-curing conditions with the highest strength and modulus.

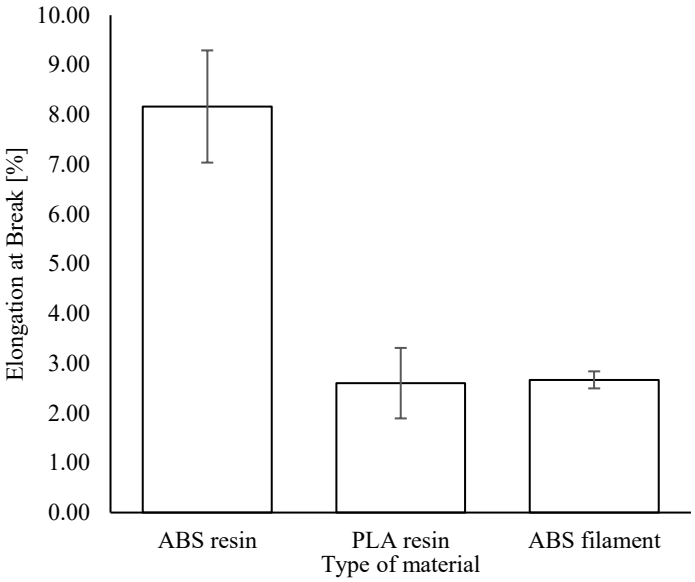

Figure 16. Elongation at break for each material

As can be seen in both Figures 15 and 16, ABS resin shows the highest ductility among the three materials, which is characterized by the elongation at break of the material. ABS resin fails at an average elongation of 8.2%, 314% greater than PLA resin. Both PLA resin and ABS filament had similar ductility. Ductile materials can absorb a large amount of energy in the plastic region before they fail [74]. Important properties for propellers include being light, strong, ductile, easy to fabricate and resistant to erosion and corrosion [74]. In this work, the propellers are used for small UAVs. Therefore, the focus is not on the strength, but on the ductility of the material. For this reason, ABS resin is chosen to fabricate the NACA4412 and Clark-Y propellers.

3.2 Static Test Results

Figure 17 shows the power required to rotate the propellers. The relationship between the power required and the propeller rotation shows a proportional pattern, and both propellers produced almost the same result from 0 to 25 W. However, at higher rotation, Clark-Y shows a lower power consumption required to generate one propeller rotation at the same speed compared to NACA 4412, with a small percentage difference. At the highest rotation speed of 22500 RPM, Clark-Y consumes 100.9 W less power than NACA 4412 at 109.5 W, a percentage difference of 8.52%. This shows that Clark-Y requires less power to operate at the same speed compared to NACA 4412.

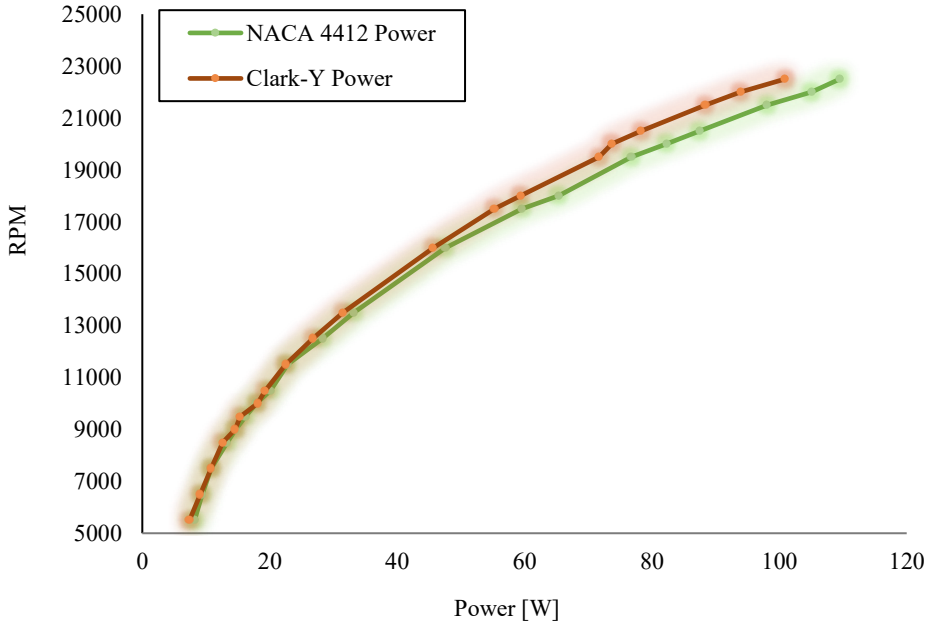

Figure 17. Power required to rotate propellers

Figure 18 represents the thrust generated as a function of propeller speed between NACA 4412 and Clark-Y. The graph shows that the thrust generated increases proportionally with the increase in RPM for both airfoil propeller shapes.

However, NACA 4412 generates higher thrust at every RPM point compared to Clark-Y and achieves the highest thrust value of 2.16 N at a maximum 22500 RPM, compared to Clark-Y at 2.06 N.

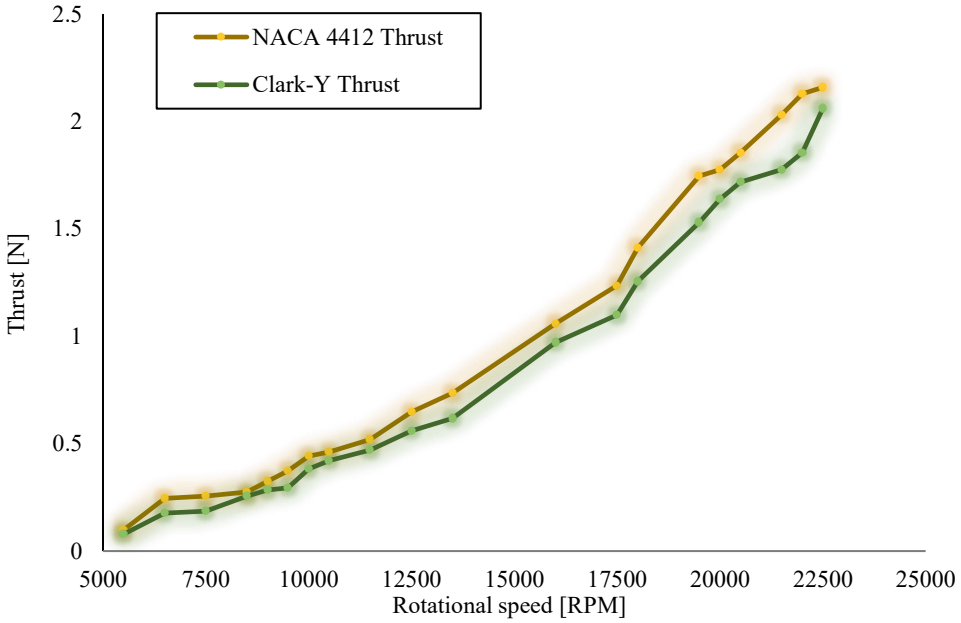

Figure 18. Thrust produced by propellers

Referring to Figure 19, the propeller with the NACA 4412 blade showed higher CT values than the Clark-Y propeller in relation to the rotational speeds. The CT of the propeller with NACA 4412 airfoil increased with an average of 15.86% compared to the Clark-Y propeller, corresponding to the rotational speed. The trend shows that the CT increases rapidly with rotational speed at the beginning and drops sharply from 6500 RPM to 7500 RPM. A further increase in rotational speed results in the CT showing a consistent pattern from 7500 ABS to the maximum rotation of 22500 RPM.

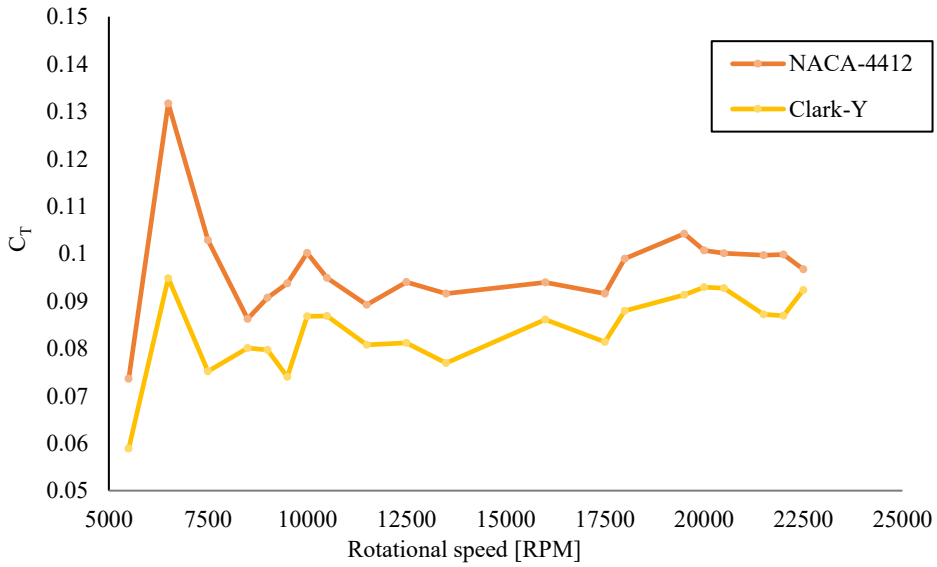

Figure 19. C_T of propellers

Meanwhile, Figure 20 shows the CP determined for NACA 4412 and Clark-Y propellers. At 7500 RPM, there is no difference between the CP of these two propellers. This means that the power consumption at this rotational speed is the same as that at the other rotational speeds. The percentage difference in CP at the other rotational speeds is less than 10%. Considering this, the NACA 4412 airfoil has a slightly better CP performance, the difference with the Clark-Y propeller is minimal.

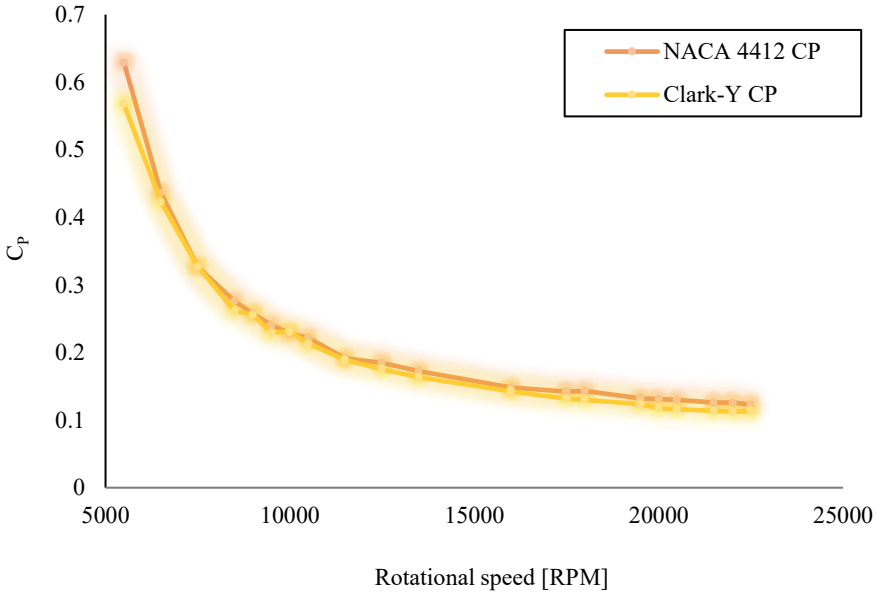

Figure 20. C_P of propellers

On the other hand, Figure 21 shows that the propeller with the NACA 4412 blade generally has a higher efficiency than the Clark-Y propeller. Ultimately, the higher CP leads to a lower efficiency, and the higher CT results in a higher efficiency or vice versa. The propeller with the NACA 4412 blade shows a higher efficiency from 5500 RPM to 19500 RPM, but the difference between the efficiencies of the propellers slowly decreases with increasing rotational speed until the Clark-Y propeller shows the highest efficiency at 22500 RPM.

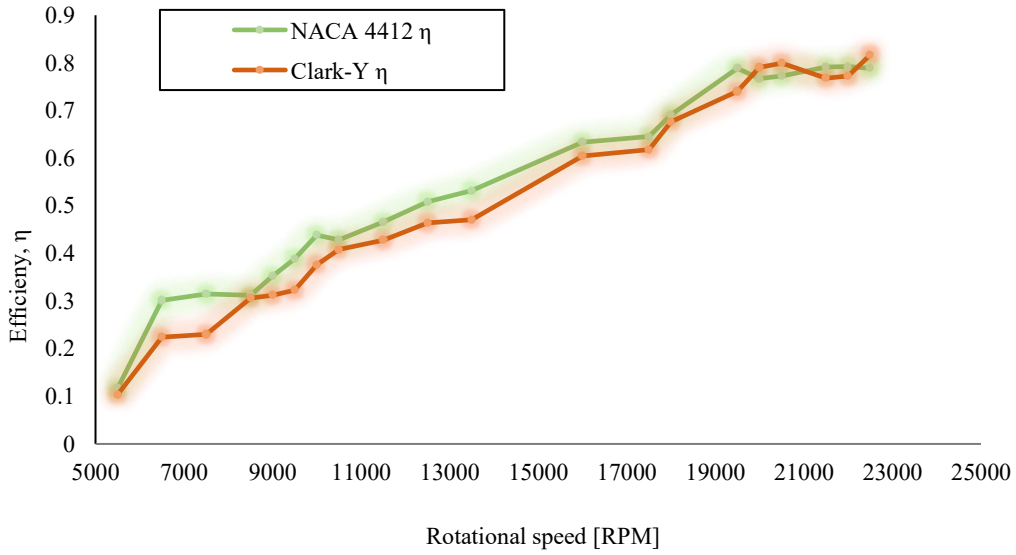

Figure 21. Efficiency of propellers

The increase in efficiency with increasing rotational speed is the most striking feature, as shown in Figure 21. A higher thrust coefficient is obtained with increased propeller speed, as can be seen from the thrust coefficient graphs. The increased thrust is most obvious as depicted in the static thrust plots. The aerodynamic performance of airfoils improves with increasing Reynolds numbers, as shown in this study and previous studies on aerodynamics at low Reynolds numbers. Extending this improved performance to propeller airfoils confirms that this trend is to be expected.

Figure 22 shows the data of the coefficient of lift (CL) versus the coefficient of drag (CD) taken at a Reynolds number of 500,000. The CD of the Clark-Y airfoil is up to 0.085 at -0.50 CL. For NACA 4412, however, the CD is only depicted up to 0.04. At CD values from 0.03 to approximately 0.085, NACA 4412 has a higher CL value, reaching up to 1.50, compared to the Clark-Y airfoil with a slightly lower CL. Since the CL and CD profiles influence the thrust, power and efficiency performance of the propeller, the generation of higher lift at a lower drag means that the NACA 4412 airfoil should perform better than the Clark-Y airfoil. Figure 23 represents the CL versus angle of attack (α) of NACA 4412 and Clark-Y at (a) 50000, (b) 200000, (c) 500000 and (d) 1000000 Reynolds number from the Airfoil plotter. It can be noticed that the NACA 4412 airfoil generally produced a higher CL value at each Reynolds number, compared to the Clark-Y

airfoil at each angle of attack. These results support that a propeller performs better aerodynamically when using an airfoil shape with a higher CL, especially in terms of the thrust produced.

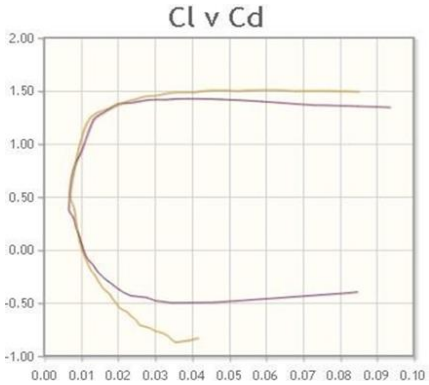

Figure 22. C_L vs C_D of NACA 4412 versus Clark-Y at 500,000 Reynolds number from Airfoil plotter

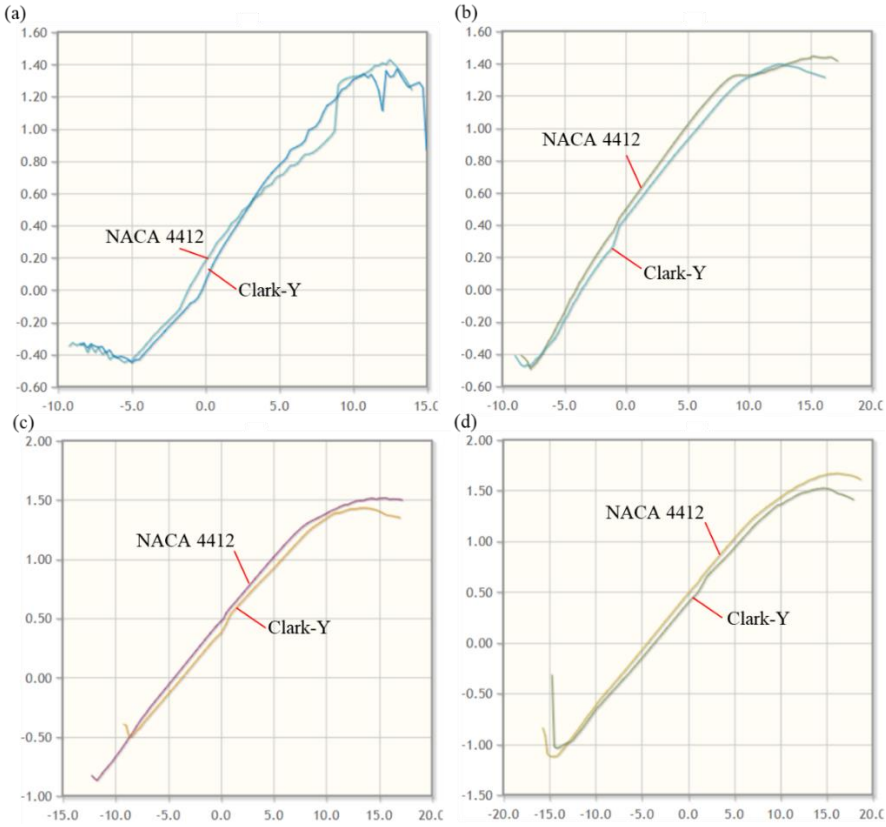

Figure 23. C_L versus α (unit: degree) of NACA 4412 and Clark-Y at (a) 50000, (b) 200000, (c) 500000 and (d) 1000000 Reynolds number from Airfoil plotter

4. CONCLUSION

In this work, the most suitable material for fabricating the propeller is determined based on the results of the tensile test. The analysis of the aspects of strength and ductility is measured and compared with ABS filament, ABS resin and PLA resin. The results show that ABS resin fulfilled the criteria for propeller material with a ductility of 9.6%.

The performance of the propeller is investigated by conducting static tests. The overall static characteristics of the propeller are measured and compared with those of the NACA 4412 airfoil-based propeller and the Clark-Y airfoil-based propeller. A complete experimental setup and the procedure for both cases are presented in this work. The comparison results of the two propellers show static thrust differences of 15.86% and 9.32% efficiency, respectively, for the respective NACA 4412 and Clark-Y propellers used in this work. However, there is a small difference in the power coefficient of15.86%, which could be due to the recorded average rotational speed of the propellers. The results have shown that propellers designed with NACA 4412 airfoil are generally more efficient with the same diameter and pitch. In the future, other experiments, such as dynamic tests, can be conducted to obtain real flight conditions, as the static performance of the blade was addressed in this work.

ACKNOWLEDGEMENTS

This research was funded by a grant from Universiti Putra Malaysia (Endowment Tan Sri Syed Azman UPM-6338207).

CONFLICT OF INTEREST

The authors declare that no conflicts of interest related to this research.

AUTHORS CONTRIBUTION

Muhammad Nor Ikmal Muhamad Nazri conducted the experimental work and contributed to the manuscript writing.

Adi Azriff Basri provided guidance on the aerodynamic aspects and assisted in writing the paper.

Mohd Na'im Abdullah and Faizal Mustapha offered expert advice on materials.

Farid Bajuri was responsible for writing the methodology section.

Ernnie Illyani Basri prepared the introduction.

Nasrul Hadi Johari contributed to the conclusion and finalization of the manuscript.

REFERENCES

[1] E. John, "Flight dynamics of an unmanned aerial vehicle," 1994. [Online]. Available: http://hdl.handle.net/10945/28222

[2] G. Hoffmann, H. Huang, S. Waslander, and C. Tomlin, "Quadrotor Helicopter Flight Dynamics and Control: Theory and Experiment," in *AIAA Guidance, Navigation and Control Conference and Exhibit*, Reston, Virginia: American Institute of Aeronautics and Astronautics, 2007.

[3] M. Khan, "Quadcopter Flight Dynamics," *International Journal of Scientific & Technology Research*, vol. 3, no. 8, pp. 130-135, 2014.

[4] V. H. Dominguez, L. A. Reyes-Osorio, J. Ollervides-Vazquez, and O. Garcia-Salazar, "Design and manufacture of a micro unmanned aerial vehicle," *Journal of Aerospace Engineering*, vol. 37, no. 1, p. 06023003, 2024.

[5] J. Choi, H. M. Kim, H. J. Hwang, Y.-D. Kim, and C. O. Kim, "Modular reinforcement learning for autonomous UAV flight control," *Drones*, vol. 7, no. 7, p. 418, 2023.

[6] P. Tong, X. Yang, Y. Yang, W. Liu, and P. Wu, "Multi-UAV collaborative absolute vision positioning and navigation: A survey and discussion," *Drones*, vol. 7, no. 4, p. 261, 2023.

[7] C. W. Park and H. T. Chung, "A study on drone charging system using wireless power transmission," 2017. [Online]. Available: www.ijtrd.com

[8] Y. Chen, D. Baek, A. Bocca, A. Macii, E. Macii, and M. Poncino, "A case for a battery-aware model of drone energy consumption," in *2018 IEEE International Telecommunications Energy Conference (INTELEC)*, IEEE, 2018, pp. 1–8.

[9] S. S. Mansouri, P. Karvelis, G. Georgoulas, and G. Nikolakopoulos, "Remaining useful battery life prediction for UAVs based on machine learning," *IFAC-PapersOnLine*, vol. 50, no. 1, pp. 4727–4732, 2017.

[10] D. Caballero-Martin, J. M. Lopez-Guede, J. Estevez, and M. Graña, "Artificial intelligence applied to drone control: A state of the art," *Drones*, vol. 8, no. 7, p. 296, 2024.

[11] S. A. H. Mohsan, N. Q. H. Othman, M. A. Khan, H. Amjad, and J. Żywiołek, "A comprehensive review of micro UAV charging techniques," *Micromachines (Basel)*, vol. 13, no. 6, p. 977, 2022.

[12] S. Bhosale, V. Jadhav, and D. Surendra Bhosale, "Battery management system for drones," in *International Conference on Electrical Electronics and Data Communication, Kolkata, India*, 2022, pp. 1-6.

[13] L. Bláha, O. Severa, M. Goubej, T. Myslivec, and J. Reitinger, "Automated drone battery management system—Droneport: Technical overview," *Drones*, vol. 7, no. 4, p. 234, 2023.

[14] J. Ragupathi, "Hydrogen fuel cell drones against battery drones: Last mile delivery persepective," School of Industrial Engineering West Lafayette, Indiana, 2023.

[15] K. Anoune, I. El Kafazi, A. El Maliki, B. Bossoufi, B. Nasiri, H. Zekraoui, et al., "Performance enhancement of drone LiB state of charge using extended Kalman filter algorithm," *Cleaner Engineering and Technology*, vol. 25, p. 100917, 2025.

[16] Y. W. Son, D. Kang, and J. Kim, "Passive battery thermal management system for an unmanned aerial vehicle using a tetrahedral lattice porous plate," *Applied Thermal Engineering*, vol. 225, p. 120186, 2023.

[17] S. Hassouna and A. Mohamed Kamal, "Parametric investigation of wing geometric characteristics for enhancing UAV endurance," in *International Conference on Aerospace Sciences and Aviation Technology*, vol. 21, no. 21, pp. 1-19, 2025.

[18] B. Vergouw, H. Nagel, G. Bondt, and B. Custers, "Drone technology: Types, payloads, applications, frequency spectrum issues and future developments," in *The future of drone use: Opportunities and threats from ethical and legal perspectives*, pp. 21-45. The Hague: TMC Asser Press, 2016.

[19] A. C. Haefner, T. L. Jones, S. W. Miller, and J. A. Cole, "Characterization of aeropropulsive performance of small unmanned aircraft system paramotor," *Journal of Aircraft*, pp. 1–12, 2025.

[20] P. Beigi, M. S. Rajabi, and S. Aghakhani, "An overview of drone energy consumption factors and models," in *Handbook of Smart Energy Systems*, Cham: Springer International Publishing, 2022, pp. 1–20.

[21] M. Saponi, A. Borboni, R. Adamini, R. Faglia, and C. Amici, "Embedded payload solutions in UAVs for medium and small package delivery," *Machines*, vol. 10, no. 9, p. 737, 2022.

[22] D. E. Martin and M. A. Latheef, "Payload capacities of remotely piloted aerial application systems affect spray pattern and effective swath," *Drones*, vol. 6, no. 8, p. 205, 2022.

[23] Y. Kim and S. Kang, "Development of optimal energy management strategy for proton exchange membrane fuel cell-battery hybrid system for drone propulsion," *Applied Thermal Engineering*, vol. 258, p. 124646, 2025.

[24] G. Quattrini, S. Pesaresi, N. Hofmann, A. Mancini, and S. Casavecchia, "Integrating drone truthing and functional classification of remote sensing time series for supervised vegetation mapping," *Remote Sens (Basel)*, vol. 17, no. 2, p. 330, 2025.

[25] J. Stewart, R. J. Francis, D. J. Eldridge, R. T. Kingsford, and N. M. de Lima, "Advancing remote sensing of biocrusts with drone imagery and machine learning," *Geoderma*, vol. 458, p. 117315, 2025.

[26] B. Gano, S. Bhadra, J. M. Vilbig, N. Ahmed, V. Sagan, and N. Shakoor, "Drone-based imaging sensors, techniques, and applications in plant phenotyping for crop breeding: A comprehensive review," *The Plant Phenome Journal*, vol. 7, no. 1, p. e20100, 2024.

[27] A. Abdusalomov, S. Umirzakova, M. B. Shukhratovich, M. Mukhiddinov, A. Kakhorov, A. Buriboev, et al., "Drone-based wildfire detection with multi-sensor integration," *Remote Sensing (Basel)*, vol. 16, no. 24, p. 4651, 2024.

[28] R. N. Sahoo, R. G. Rejith, S. Gakhar, R. Ranjan, M. C. Meena, A. Dey, et al., "Drone remote sensing of wheat N using hyperspectral sensor and machine learning," *Precision Agriculture*, vol. 25, no. 2, pp. 704–728, 2024.

[29] S. S. Jayakumar, I. P. Subramaniam, B. S. Arputharaj, S. K. Solaiappan, P. Rajendran, I. E. Lee, et al., "Design, control, aerodynamic performances, and structural integrity investigations of compact ducted drone with co-axial propeller for high altitude surveillance," *Scientific Reports*, vol. 14, no. 1, p. 6330, 2024.

[30] P. D. Bravo-Mosquera, L. Botero-Bolivar, D. Acevedo-Giraldo, and H. D. Cerón-Muñoz, "Aerodynamic design analysis of a UAV for superficial research of volcanic environments," *Aerospace Science and Technology*, vol. 70, pp. 600–614, 2017.

[31] R. Morishita, S. Kawai, and H. Nobuhara, "Downwash reduction drone with adaptive rotors and its 3D aerodynamic analysis and stabilization control," *IEEE Access*, vol. 12, pp. 22832–22840, 2024.

[32] D. Shukla and N. Komerath, "Multirotor drone aerodynamic interaction investigation," *Drones*, vol. 2, no. 4, p. 43, 2018.

[33] S. Prothin, C. Fernandez Escudero, N. Doué, and T. Jardin, "Aerodynamics of MAV rotors in ground and corner effect," *International Journal of Micro Air Vehicles*, vol. 11, p.1756829319861596, 2019.

[34] C. Paz, E. Suárez, C. Gil, and C. Baker, "CFD analysis of the aerodynamic effects on the stability of the flight of a quadcopter UAV in the proximity of walls and ground," *Journal of Wind Engineering and Industrial Aerodynamics*, vol. 206, p. 104378, 2020.

[35] S. Krishnaraj, R. Senthil Kumar, A. Gokula Krishnan, G. Ganeshkumar, M. Mohan, and M. Nirmal, "Aerodynamic analysis of hybrid drone," *IOP Conference Series: Materials Science and Engineering*, vol. 1012, no. 1, p. 012023, 2021.

[36] L. S. Sawaqed, A. H. Bani Younes, and M. I. Aldalal'ah, "Aerodynamics effect of holes in UAV wings modified for VTOL capability," *Drone Systems and Applications*, vol. 10, no. 1, pp. 330–342, 2022.

[37] K. Anuar, M. Akbar, H. A. Aziz, and A. Soegihin, "Experimental test on aerodynamic performance of propeller and its effect on the flight performance of Serindit V-2 UAV," *Journal of Advanced Research in Fluid Mechanics and Thermal Sciences*, vol. 91, no. 2, pp. 120–132, 2022.

[38] E. Gallo, J. De Decker, A. Bresciani, P. Haezebrouck, E. Garone, and C. Schram, "Development and commissioning of an aeroacoustic test bench for the investigation of single and coaxial propeller noise," *Acta Acustica*, vol. 9, p. 16, 2025.

[39] R. S. McKay, M. J. Kingan, S. T. Go, and R. Jung, "Experimental and analytical investigation of contra-rotating multi-rotor UAV propeller noise," *Applied Acoustics*, vol. 177, p. 107850, 2021.

[40] W. Song, Z. Mu, Y. Wang, Z. Zhang, S. Zhang, Z. Wang, et al., "Comparative investigation on improved aerodynamic and acoustic performance of abnormal rotors by bionic edge design and rational material selection," *Polymers (Basel)*, vol. 14, no. 13, p. 2552, 2022.

[41] F. Li and O. Kunze, "A comparative review of air drones (UAVs) and delivery bots (SUGVs) for automated last mile home delivery," *Logistics*, vol. 7, no. 2, p. 21, 2023.

[42] S. Chiesa, S. Farfaglia, M. Fioriti, and N. Viola, "Design of all electric secondary power system for future advanced medium altitude long endurance unmanned aerial vehicles," *Proceedings of the Institution of Mechanical Engineers, Part G*, vol. 226, no. 10, pp. 1255–1270, 2012.

[43] L. Cwojdziński and M. Adamski, "Power units and power supply systems in UAV," *Aviation*, vol. 18, no. 1, pp. 1–8, 2014.

[44] M. Krznar, P. Piljek, D. Kotarski, and D. Pavković, "Modeling, control system design and preliminary experimental verification of a hybrid power unit suitable for multirotor UAVs," *Energies (Basel)*, vol. 14, no. 9, p. 2669, 2021.

[45] A. Townsend, I. N. Jiya, C. Martinson, D. Bessarabov, and R. Gouws, "A comprehensive review of energy sources for unmanned aerial vehicles, their shortfalls and opportunities for improvements," *Heliyon*, vol. 6, no. 11, p. e05285, 2020.

[46] K. L. Pham, J. Leuchter, R. Bystricky, M. Andrle, N. N. Pham, and V. T. Pham, "The study of electrical energy power supply system for UAVs based on the energy storage technology," *Aerospace*, vol. 9, no. 9, p. 500, 2022.

[47] W. Zhou, K. Yin, R. Wang, and Y.-E. Wang, "Design of attitude control system for UAV based on feedback linearization and adaptive control," *Mathematical Problems in Engineering*, vol. 2014, no. 1, p. 492680, 2014.

[48] M. Jafari and H. Xu, "Intelligent control for unmanned aerial systems with system uncertainties and disturbances using artificial neural network," *Drones*, vol. 2, no. 3, p. 30, 2018.

[49] V. Kangunde, R. S. Jamisola, and E. K. Theophilus, "A review on drones controlled in real-time," *International Journal of Dynamics and Control*, vol. 9, no. 4, pp. 1832–1846, 2021.

[50] D. D. Nguyen, J. Rohacs, and D. Rohacs, "Autonomous flight trajectory control system for drones in smart city traffic management," *ISPRS International Journal of Geo-Information*, vol. 10, no. 5, p. 338, 2021.

[51] M. W. Mueller, S. J. Lee, and R. D'Andrea, "Design and control of drones," *Annual Review of Control, Robotics, and Autonomous Systems*, vol. 5, no. 1, pp. 161–177, 2022.

[52] S.-W. Chen, Y.-C. Lai, C.-T. Tsai, C.-H. Liu, and J.-F. Tu, "Development of intelligent drone remote control system based on internet of things," *Sensors and Materials*, vol. 34, no. 7, p. 2581, 2022.

[53] Y. L. Yap, W. Toh, A. Giam, F. R. Yong, K. I. Chan, J. W. S. Tay, et al., "Topology optimization and 3D printing of micro-drone: Numerical design with experimental testing," *International Journal of Mechanical Sciences*, vol. 237, p. 107771, 2023.

[54] Y. L. Yap, W. Toh, R. Koneru, K. Lin, K. M. Yeoh, C. M. Lim, et al., "A non-destructive experimental-cum-numerical methodology for the characterization of 3D-printed materials—polycarbonate-acrylonitrile butadiene styrene (PC-ABS)," *Mechanics of Materials*, vol. 132, pp. 121–133, 2019.

[55] K. Agarwal, S. K. Kuchipudi, B. Girard, and M. Houser, "Mechanical properties of fiber reinforced polymer composites: A comparative study of conventional and additive manufacturing methods," *Journal of Composite Materials*, vol. 52, no. 23, pp. 3173–3181, 2018.

[56] P. Pecho, V. Ažaltovič, B. Kandera, and M. Bugaj, "Introduction study of design and layout of UAVs 3D printed wings in relation to optimal lightweight and load distribution," *Transportation Research Procedia*, vol. 40, pp. 861–868, 2019.

[57] Y. Vashi, R. Anand, K. Jayakrishna, G. Rajyalakshmi, and S. A. Raj, "Design and analysis of 3D printed UAV wheel," *Materials Today: Proceedings*, vol. 46, pp. 8307–8312, 2021.

[58] N. Muralidharan, V. G. Pratheep, A. Shanmugam, A. Hariram, P. Dinesh, and B. Visnu, "Structural analysis of mini drone developed using 3D printing technique," *Materials Today: Proceedings*, vol. 46, pp. 8748–8752, 2021.

[59] S. Schröder, C. D. Grimm, L. Witte, A. Dimassi, and P. Buchholz, "Design, development and testing of 3D-printed conformal energy absorbing structures," *Materials Today Communications*, vol. 35, p. 106204, 2023.

[60] V. S. R. P. Akula, S. Basu, K. K. Goyal, O. P. Verma, V. Gupta, and V. Srivastava, "Efficiency takes flight: 3D-Printed A2212 brushless direct current outrunner motor propelling next-gen drone deliveries," *Journal of Materials Engineering and Performance*, vol. 34, no. 16, pp. 17185–17194, 2025.

[61] M. A. M. Mabbrur, H. E. A. N. P., N. S. Syaifer, A. Hidayat, and S. F. Nadzir, "UAV wing structure with 3D printed PLA filament wing spar," *International Journal of Mechanical Engineering and Robotics Research*, vol. 9, no. 3, pp. 464–469, 2020.

[62] G. L. Goh, V. Dikshit, R. Koneru, Z. K. Peh, W. Lu, G. D. Goh, et al., "Fabrication of design-optimized multifunctional safety cage with conformal circuits for drone using hybrid 3D printing technology," *The International Journal of Advanced Manufacturing Technology*, vol. 120, no. 3–4, pp. 2573–2586, 2022.

[63] S. Brischetto, C. Ferro, P. Maggiore, and R. Torre, "Compression tests of ABS specimens for UAV components produced via the FDM technique," *Technologies (Basel)*, vol. 5, no. 2, p. 20, 2017.

[64] H. Agarwal, A. Singhal, and K. H. Raj, "3D Printed Quadcopter," in *Advances in Systems Engineering: Select Proceedings of NSC 2019*, pp. 491-499, 2021.

[65] R. Deters, *UIUIC Propeller Database - Volume 2*, Department of Aerospace Engineering, University of Illinois at Urbana-Champaign, 2015.

[66] R. W. Deters, G. K. Ananda Krishnan, and M. S. Selig, "Reynolds number effects on the performance of small-scale propellers," in *32nd AIAA Applied Aerodynamics Conference*, Reston, Virginia: American Institute of Aeronautics and Astronautics, 2014.

[67] R. Deters and M. Selig, "Static testing of micro propellers," in *26th AIAA Applied Aerodynamics Conference*, Reston, Virigina: American Institute of Aeronautics and Astronautics, 2008.

[68] K. Szykiedans and W. Credo, "Mechanical properties of FDM and SLA low-cost 3-D Prints," *Procedia Engineerin*, vol. 136, pp. 257–262, 2016.

[69] A. Alhamed, "What are shells in 3D printing?" Cytron Technologies, 2023. [Online] https://my.cytron.io/tutorial/what-are-shells-in-3-d-printing

[70] F. Cosmi and A. Dal Maso, "A mechanical characterization of SLA 3D-printed specimens for low-budget applications," *Materials Today: Proceedings*, vol. 32, pp. 194–201, 2020.

[71] C. Riccio, M. Civera, O. Grimaldo Ruiz, P. Pedullà, M. Rodriguez Reinoso, G. Tommasi, et al., "Effects of curing on photosensitive resins in SLA additive manufacturing," *Applied Mechanics*, vol. 2, no. 4, pp. 942–955, 2021.

[72] *IARC Working Group on the Evaluation of Carcinogenic Risks to Humans*, vol. 100. International Agency for Research on Cancer, 2012. Accessed: Sep. 01, 2025. [Online]. Available: https://www.ncbi.nlm.nih.gov/books/NBK304366/

[73] C. García-Gascón, P. Castelló-Pedrero, and J. A. García-Manrique, "Minimal surfaces as an innovative solution for the design of an additive manufactured solar-powered unmanned aerial vehicle (UAV)," *Drones*, vol. 6, no. 10, p. 285, 2022.

[74] M. M. Uddin, M. P. Hossen, M. M. Jahan, and M. I. Islam, "Structural analysis of composite propeller of ship using FEM," vol. 2324, no. 1, p. 030001 2021.